Engineering and Technology Journal
Journal homepage: https://etj.uotechnology.edu.iq

Numerical Simulation of the Self-Imaging at Different Cascaded Optical Fiber Specifications

Shahad I. Younus[a]*, Anwaar A Al-Dergazly[b] , Abdulla K. Abass [c]

[a,c]Laser and Optoelectronic Engineering Dept., University of Technology-Iraq, Alsina'a street, 10066 Baghdad, Iraq.
[b] Laser and Optoelectronic Engineering Department, Al-Naharain University, Baghdad, Iraq.
*Corresponding author Email: 140178@student.uotechnology.edu.iq

HIGHLIGHTS

- Multimode interference and self-imaging in the cascaded SNS fiber have been investigated numerically via COMSOL Multiphysics 5.5.
- To get high self-imaging quality, it is not necessary to be restricted to the rule of P = 4, 8...
- The BEM is effective in studying the field propagation in large guiding photonic devices.

ARTICLE INFO

Handling editor: Ivan A. Hashim

Keywords:
Beam envelope method
Cascaded optical fiber; Multimode interference
Self-imaging position

ABSTRACT

Cascaded optical fiber single mode-no core-single mode fiber (SNS) attracted attention for being the base of various photonic devices. These devices are used in optical communication, fiber sensors, and fiber laser technology. The effect of variable NCF specifications, length, diameter, external refractive index (ERI), propagating wavelength on the self-imaging position, and the multimode interference (MMI) is studied. The study aims to simulate and analyze cascaded optical fiber by using the finite element beam envelope method (BEM). To the best of our knowledge, this is the first report that studied the self-imaging in cascaded optical fiber longitudinally by using BEM. The NCF length is important in determining the coupled out intensity and peak transmission wavelength. The field in the cascaded fiber is simulated for single and multi-wavelengths to evaluate the maximum transmission and study the structure's tunability. A tunable filter is simulated, where varying the length of the NCF about 0.6 mm produces a wavelength shift of about 40 nm. The BEM is effective in studying the field propagation in large guiding photonic devices.

1. Introduction

Multimode Interferences (MMI) devices consist of multimode fiber (MMF). In certain applications, a No Core Fiber (NCF) connected between two Single-Mode Fiber (SMF) MMI attracted attention. Their important preference is compact, easily fabricating, low loss, and cost-effective. MMI occurs when the fundamental mode of the SMF transfers to the MMF. The modes in MMF are exited and interfere as they propagate along with the fiber, giving an interference pattern. At certain positions along with the MMF, the waves constructively interfere, forming a replication of the entrance field named self-imaging. The cascaded fiber device is used as a tunable filter [1], [2] bandpass filter [3], [4], and fiber sensor [5]–[7].

MMI and the self-imaging effect are firstly demonstrated in a planar waveguide. It is used widely in designing high-efficiency waveguide couplers [8]. MMI is more sophisticated than in a planar waveguide in an optical fiber. It is firstly observed in fiber by Allison in [9]. MMI and self-imaging effect is also used in the active multimode waveguide (MMW) to obtain single-mode emission from a planner MMW [10]. A fiber laser based on MMI generating single-mode emission from MMF has been demonstrated [11]. The first tunable fiber laser based on the MMI filter was introduced by Selvas in 2005 [12]. The tuning mechanism is realized by varying the distance between the MMF end facet and a broadband metallic mirror.

The tunability was 8 nm. The technique was developed to increase the tunability and stability of the system. In 2019, X. Lian et al. [13] studied the self-imaging in cladding modes of the small core optical fiber for the first time. The results show that the cladding self-imaging period grows exponentially with the core size. The study brings new insight into the field propagation in the fiber with a core at the nano/microscale, Jing et al. [14] demonstrate a continuous tuning of Optical Parametric Oscillation (OPO) from 1655.4 to 1642.5 nm by two cascade SMS structures spliced in the ring cavity as a tunable filter due to the low loss of the structure. A tuning was 12.9 nm by stretching the structure. Recently, F. Mangini et al. [15] experimentally studied the

http://doi.org/10.30684/etj.v40i2.2236
Received 16 June 2021; Accepted 13 August 2021; Available online 25 February 2022
2412-0758/University of Technology-Iraq, Baghdad, Iraq

self-imaging in few-mode fiber and SMF. Intense IR pulses excite visible luminescence via a multiphoton absorption mechanism. The study determines the mode propagation constant and the cut-off wavelength of the transverse modes. In this work, the finite element method (FEM) is used to simulate the field propagation of the MMI and the self-imaging in the cascaded optical fiber. The study illustrates the working principle of the MMI fiber device and the parameters that affect the device's performance. The effect of variable NCF length, diameter, external refractive index (ERI), and the propagated wavelength is studied. The tunability of the device is demonstrated depending on the MMI effect. To the best of our knowledge, this is the first report that studied the self-imaging in cascaded optical fiber longitudinally by using FEM. Various types of photonic devices can be designed and fabricated by characterizing the self-imaging and the MMI in NCF, used in different applications from sensing to tuning laser wavelength.

2. Theory

2.1 The self-imaging in Cascaded optical fiber

An NCF is connected between two SMF, as shown in Figure 1. The propagating field in the SMF-NCF interface decomposes into the NCF modes. The input field is reproduced at certain positions on the axis along the NCF. Only the imaging mode coupled to the NCF- SMF interface passed the MMI device.

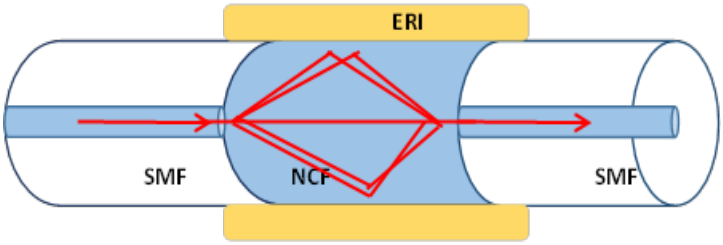

Figure 1: Schematic of the studied SNS structure

According to the theory of the MMI, the peak transmission wavelength of the MMI device is obtained as [3]

$$\lambda_\circ = \mathrm{P}\frac{\mathrm{n_1\, D_{NCF}^2}}{\mathrm{L_{NCF}}} \tag{1}$$

Where n_1 is the NCF RI, D_{NCF}, and L_{NCF} is the diameter and the length of the NCF, and P is an integer number that represents the self-imaging order. The formula indicates that when a multi-wavelength passed the MMI device, only the center wavelength ($\boldsymbol{\lambda_\circ}$) will pass. Most researchers used L equivalent to the fourth self-imaging position or its multiplications, at P = 4, 8... as real imaging with high self-imaging quality is obtained [16]. The MMI in the optical fiber agrees to the principle of symmetric interference. Only circular symmetry modes (LP_{0m}) exited [17]. Since the input field of the SMF is circularly symmetric, an SMF spliced to an MMF is perfectly aligned. The cladding RI is not included in eq. **(1)**. A study was performed to include the cladding RI [18]. The guided modes in the fiber core area are affected by the ERI. The effect is interpreted by the Evanescent Wave (EW) phenomenon. The EW is generated at the core and medium interface and penetrates the medium. The penetration depth ($\boldsymbol{d_p}$) is given by [19].

$$\mathrm{d_p} = \frac{\boldsymbol{\lambda}}{\mathbf{2\pi n_{NCF}}\sqrt{\mathbf{\sin^2\vartheta} - \left(\frac{\mathbf{n_m}}{\mathbf{n_{NCF}}}\right)^2}} \tag{2}$$

Where ϑ is the incident angle, n_{NCF} is the RI of the NCF, n_m is the ERI, the MMI eq. **(1)** become [20]

$$\lambda_\circ = \mathrm{P}\frac{\mathrm{n_1\,(D_{NCF}+2d_p)^2}}{\mathrm{L_{NCF}}} \tag{3}$$

The equation above indicates that the effective core diameter become $(D_{NCF} + 2d_p)$ which causes a shift in the wavelength. An important merit of the MMI device is that the wavelength can be designed easily to be equivalent to the required applications**.** The wavelength can be tuned by altering the ERI, the NCF length, and diameter.

To design all-fiber SNS, the length of the NCF is required to evaluate precisely. A maximum transmission occurs when the NCF length at the self-imaging position. If the coupling to the lead out SMF at the self-imaging length and a single wavelength propagation, the cascaded SNS operates as a bandpass filter. For multi-wavelength propagation, varying the length of the NCF, the peak wavelength of the filter is tuned, and thus, the range of wavelength the filter response is altered. The length is altered either by the strain effect or using index matching liquid [21]–[23].

From Eq. **(1)**, the wavelength can be controlled by the NCF specifications used in tuning applications. A length of the NCF was selected to choose the central transmitted wavelength. the relation between the length change and the shift in the wavelength is found as [24]

$$\frac{\Delta\lambda}{\lambda} = \frac{\Delta L}{L} \quad (4)$$

The wavelength shift ($\Delta\lambda$) is directly related to the NCF length variation (ΔL).

2.2 Simulation procedure

The numerical approach used the BEM explained in the previous work [25]. A 2D finite element-based model constructed in Wave Optics Module. The simulation includes two steps. First, the mode analysis study is carried out in the fiber's cross-section to determine the effective refractive indices (n_{eff}) of the fundamental mode. Second, the optical wave, beam envelope/wavelength domain study is performed to describe light propagation along with the cascaded fiber. The studied parameters are illustrated in Table (1).

Table 1: The studied parameters of the NCF and the SMF

The simulated parameter	Value
Wavelength (µm)	1.55, 1.31, 0.808, 0.65, 0.405
NCF Diameter (µm)	125, 80, 60, 40
ERI	1, 1.33, 1.36, 1.4, 1.44
NCF Length (cm)	0.7, 1.4, 3
NCF RI	1.444
SMF cladding RI	1.423
SMF core RI	1.444
SMF Diameter (µm)	8

3. Simulation results

3.1 Self-imaging position at Different wavelengths

In this section, the MMI in the cascaded fiber is studied at the wavelengths 1550, 1310, 808, 650, and 405 nm for 40 µm and 2.5 cm NCF diameter and length. The self-imaging quality, which represents the peak of the electric field at the self-imaging position, is also observed in this section. The propagation field is illustrated in Figure 2- 4. As the wavelength increases, the self-imaging order increases, and the length is reduced due to the reduction in the number of excited modes in the NCF section. The fourth self-imaging length is about 2.32, 1.12, and 0.6 cm for the 405, 808, and 1550 nm wavelengths, respectively. The self-imaging quality is one for the wavelengths 405, 650, and 808 nm, Figure 2 (c), (d) and Figure 3 (c), while it is reduced for the wavelengths 1310 and 1550 nm, Figure 3 (d) and Figure 4 (b), as the EW increased with the longer wavelength as shown in eq. (**2**). The simulation exhibits no difference in the self-imaging quality at P = 4, 8… as the previous studies used the beam propagation method (BPM), which used approximations in solving the wave equation in long guiding structures [26].

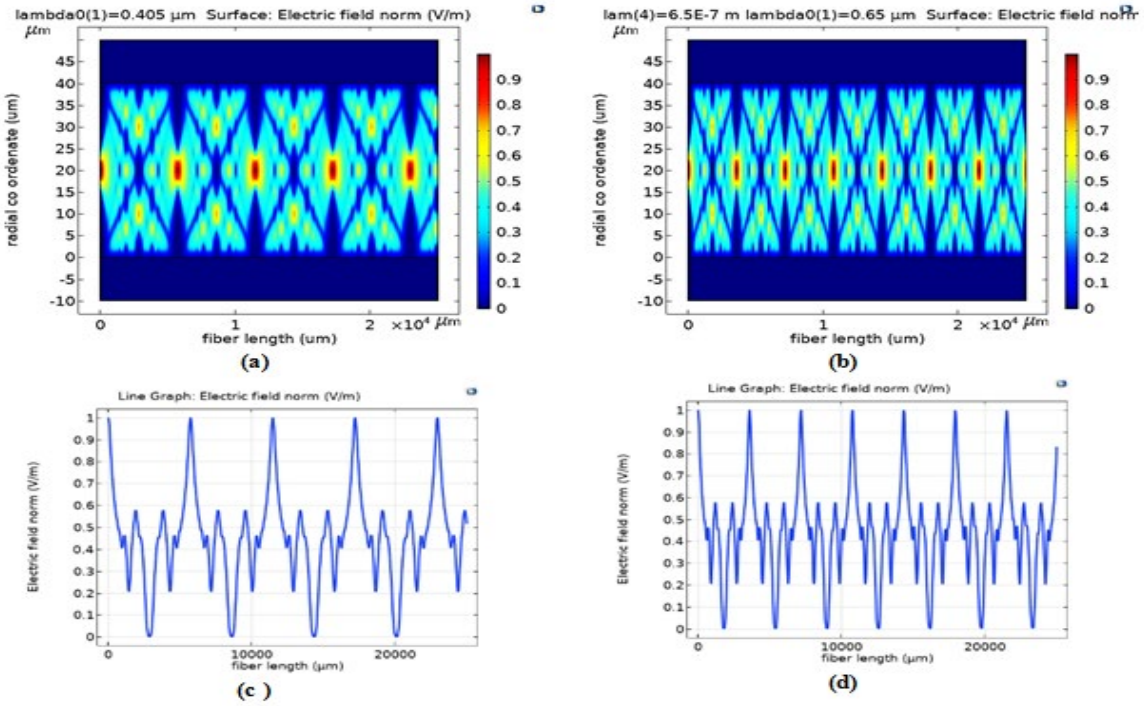

Figure 2: The MMI and the electric field illustrates the self-imaging positions for the wavelengths (a) and (c) 405 nm, (b) and (d) 650 nm wavelength, at 40 µm and 2.5 cm NCF diameters and length

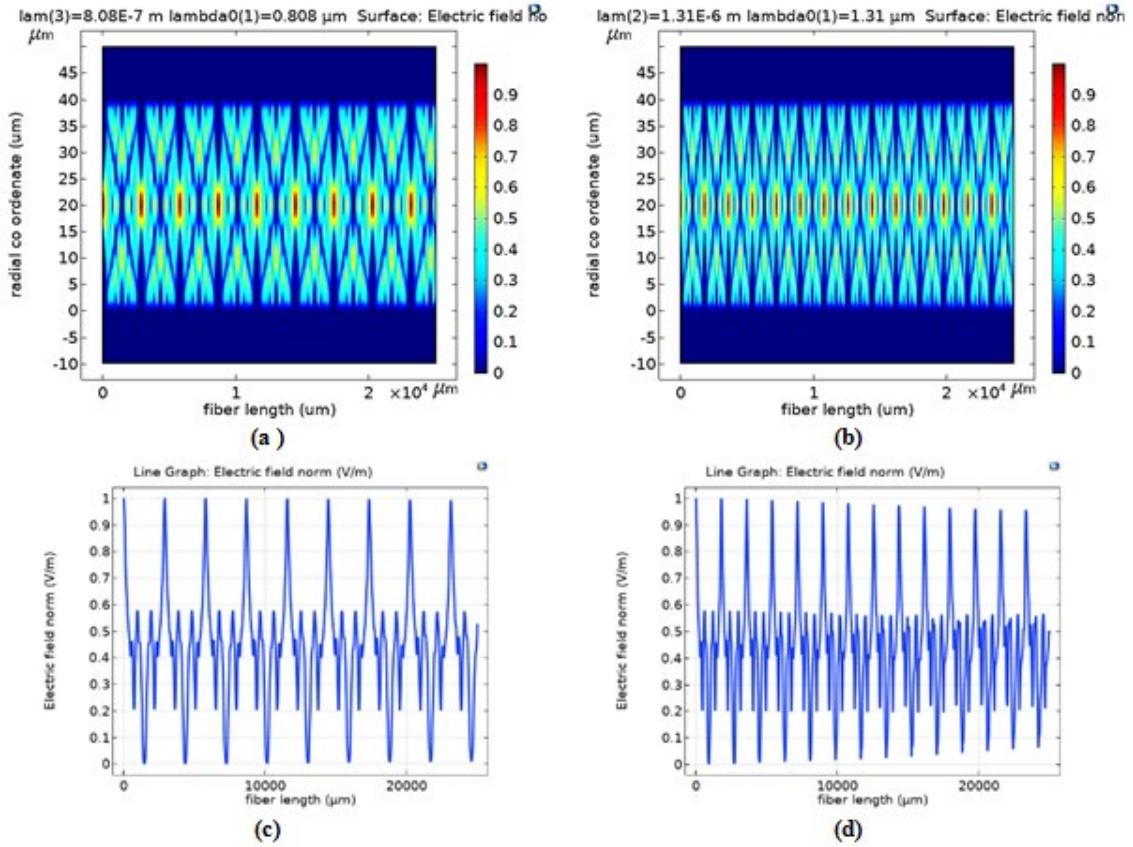

Figure 3: The MMI and the electric field profile illustrates the self-imaging positions for (a) and (c) 808 nm and (b) and (d) 1310 nm wavelength, at 40 µm and 2.5 cm NCF diameters and length

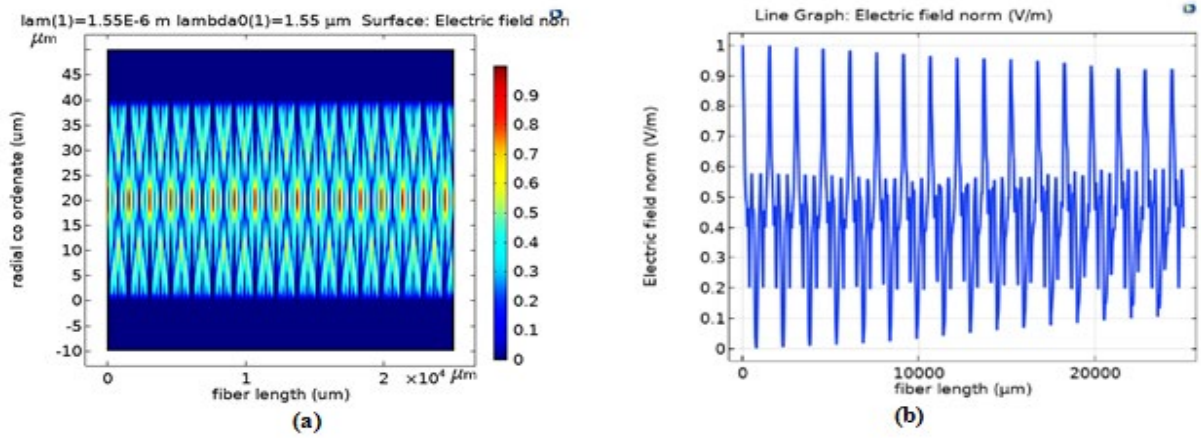

Figure 4: (a) The MMI and (b) the electric field profile illustrates the self-imaging positions for 1550 nm wavelength at 40 µm and 2.5 cm NCF diameters and length

3.2 Self-imaging position at Different NCF diameters

The MMI in the cascaded fiber at the NCF diameters 125, 80, 60, and 40 µm for 1550 nm wavelength and 6 cm NCF length is studied. In Figures 5 and 6, as the core size decreases, the self-imaging order increases and the self-imaging length reduces due to less excited modes [27]. The fourth self-imaging length of the 125 µm diameter is about 5.8 cm, and that of the 40 µm NCF fiber diameter is about 0.6 cm. The first value agrees with the literature work of [28] and [29]. The relation between the NCF diameter and the self-imaging length is quadratic, as shown in Eq. (1). The fourth self-imaging quality is about 0.85, 0.92, 0.96, and 0.99 for 125, 80, 60, and 40 µm NCF diameters, respectively. The aberration in self-imaging quality for the large NCF diameter is due to the increase in the number of excited modes, not all the interfered modes in phase [27]. The simulation exhibits no difference in self-imaging quality at P = 4, 8. The values of the fourth self-imaging length of the NCF with the diameter at different wavelengths are recorded and plotted in Table 2 and Figure 7.

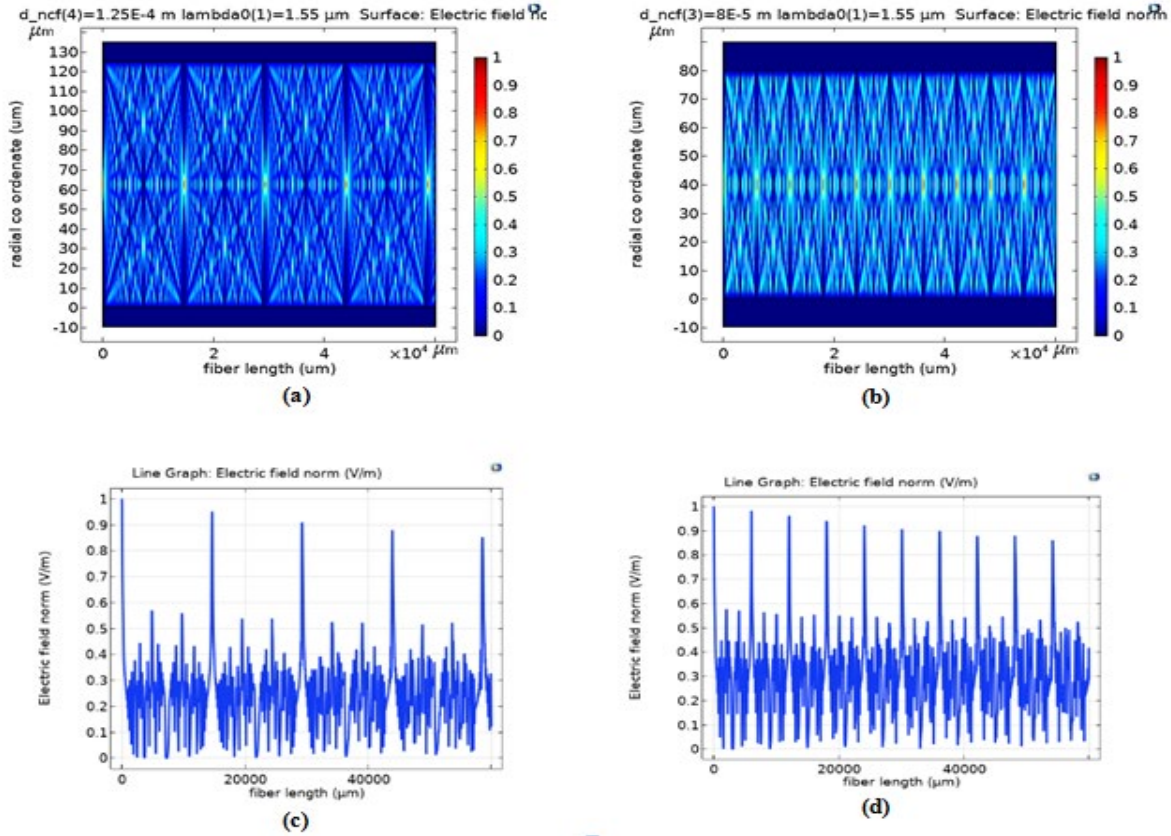

Figure 5: The MMI and the electric field illustrate the self-imaging positions at the NCF diameters (a) and (c) 125 µm, (b) and (d) 80 µm, for 1550 nm wavelength and 6 cm NCF length

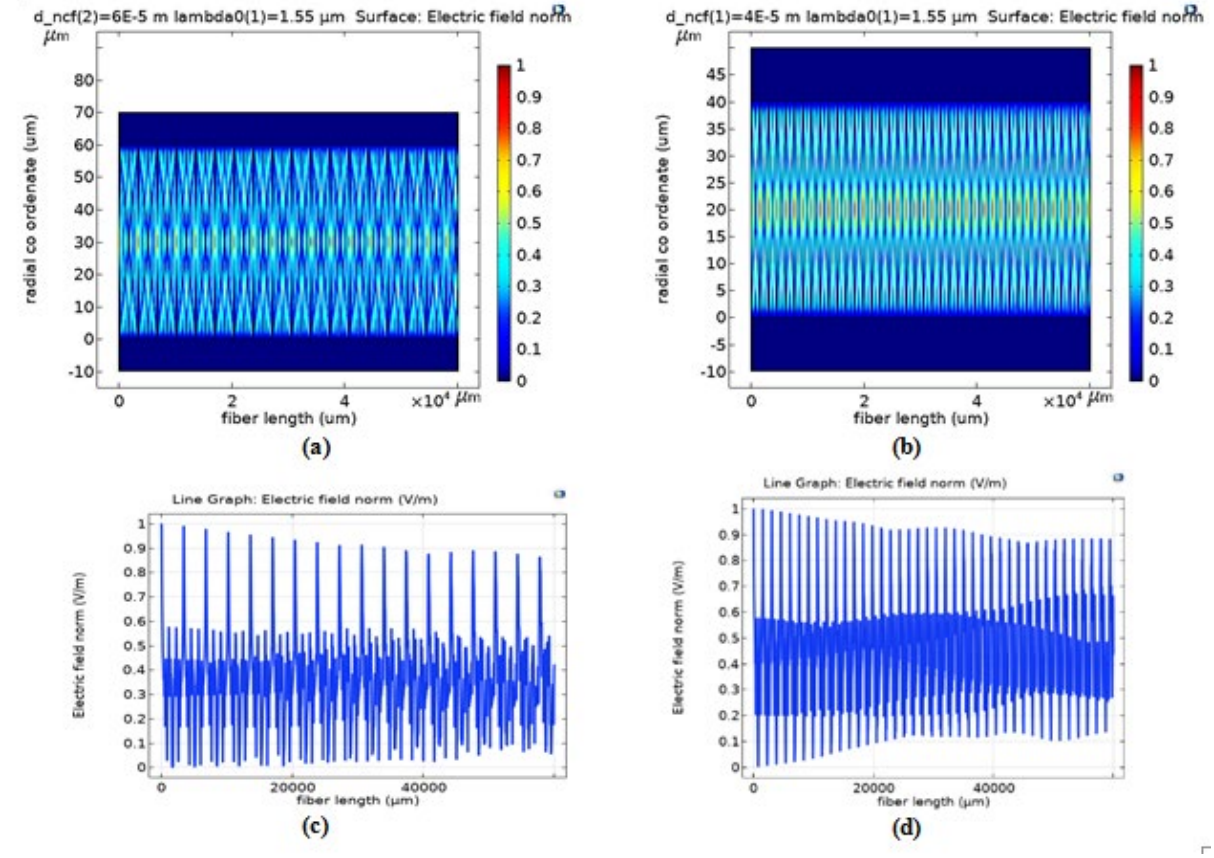

Figure 6: The MMI and the electric field illustrates the self-imaging positions at NCF diameters (a) and (c) 60 µm, (b) and (d) 40 µm, for 1550 nm wavelength and 6 cm NCF length

Table 2: The fourth self-imaging length for the diameters 40, 60, 80 and 125 µm at the wavelengths 1550, 1310, 808, 650 and 405 nm

Wavelength (nm)	The 4th self-imaging length of the NCF in (cm)			
	D = 40 µm	*D = 60 µm*	*D = 80 µm*	*D = 125 µm*
1550	0.608	1.34	2.38	5.8
1310	0.7	1.584	2.812	6.88
808	1.12	2.48	4.56	11.2
650	1.42	3.2	5.68	13.88
405	2.32	5.12	9.12	22.28

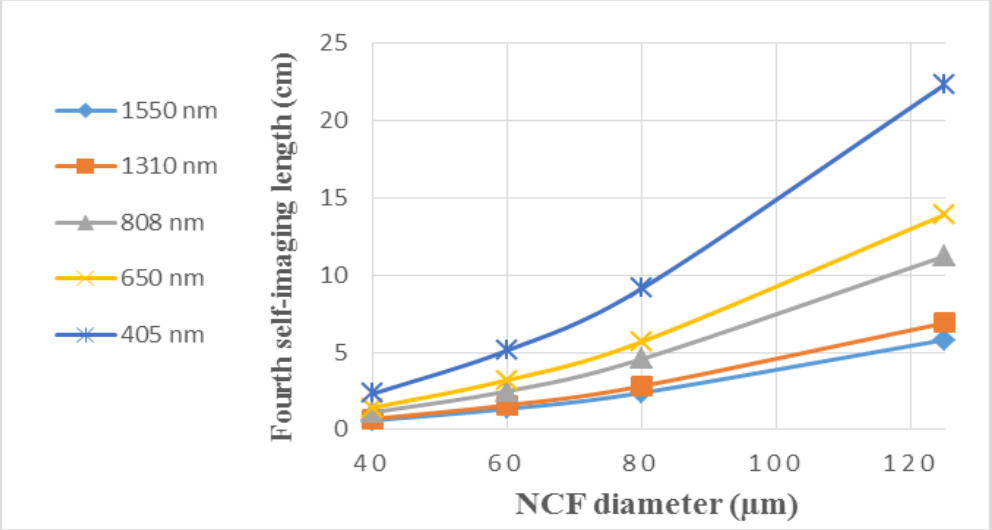

Figure 7: The fourth self-imaging length for the diameters 40, 60, 80, and 125 µm at the wavelengths 1550, 1310, 808, 650, and 405 nm

3.3 Self-imaging position at Different external refractive index (ERI)

In this section, the shift in the self-imaging position due to ERI change at the wavelengths 1550, 1310, and 808 nm for the diameters 40, 60, and 80 µm is studied. Figure 8 (a) illustrates the MMI, a maximum transmission intensity evaluated at ERI n_m = 1. Figure 8 (b) shows the transmission attenuated and the self-imaging position shift about 304 µm at ERI n_m = 1.4. Figure 8 (c) illustrates the self-imaging position of both ERI. From Figure 8, the NCF length is chosen to allow a maximum transmission at that length. The transmission with different ERI produces a shift in the MMI. The length of the self-imaging increased due to the increase in the effective refractive index [30]. The shift values in the fourth self-imaging position for the studied structure are recorded in Table 3. The shift in the self-imaging position for the wavelengths 1550 and 808 nm is about 304 and 283 µm, respectively. The shift in the self-imaging position was directly related to the wavelength since the penetration depth (d_p) increased, as shown in eq. (2). With the diameter variation, the shift for the 80 and 40 µm NCF diameter is about 573 and 304 µm, respectively. As the RI of the external medium increase, the penetration depth (d_p) expands, and the diameter becomes ($D + 2d_p$). Consequently, the self-imaging length is increased.

Table 3: The values of the shift in the fourth self-imaging position for the diameters 40, 60, and 80 µm at the wavelengths 1550, 1310, and 808 nm due to the change in ERI from 1 to 1.4

Wavelength (nm)	The shift in the 4th self-imaging position at ERI change from 1 to 1.4 in (µm)		
	D = 40 µm	*D = 60 µm*	*D = 80 µm*
1550	304.7	438	573
1310	296	433	568
808	283	425	558

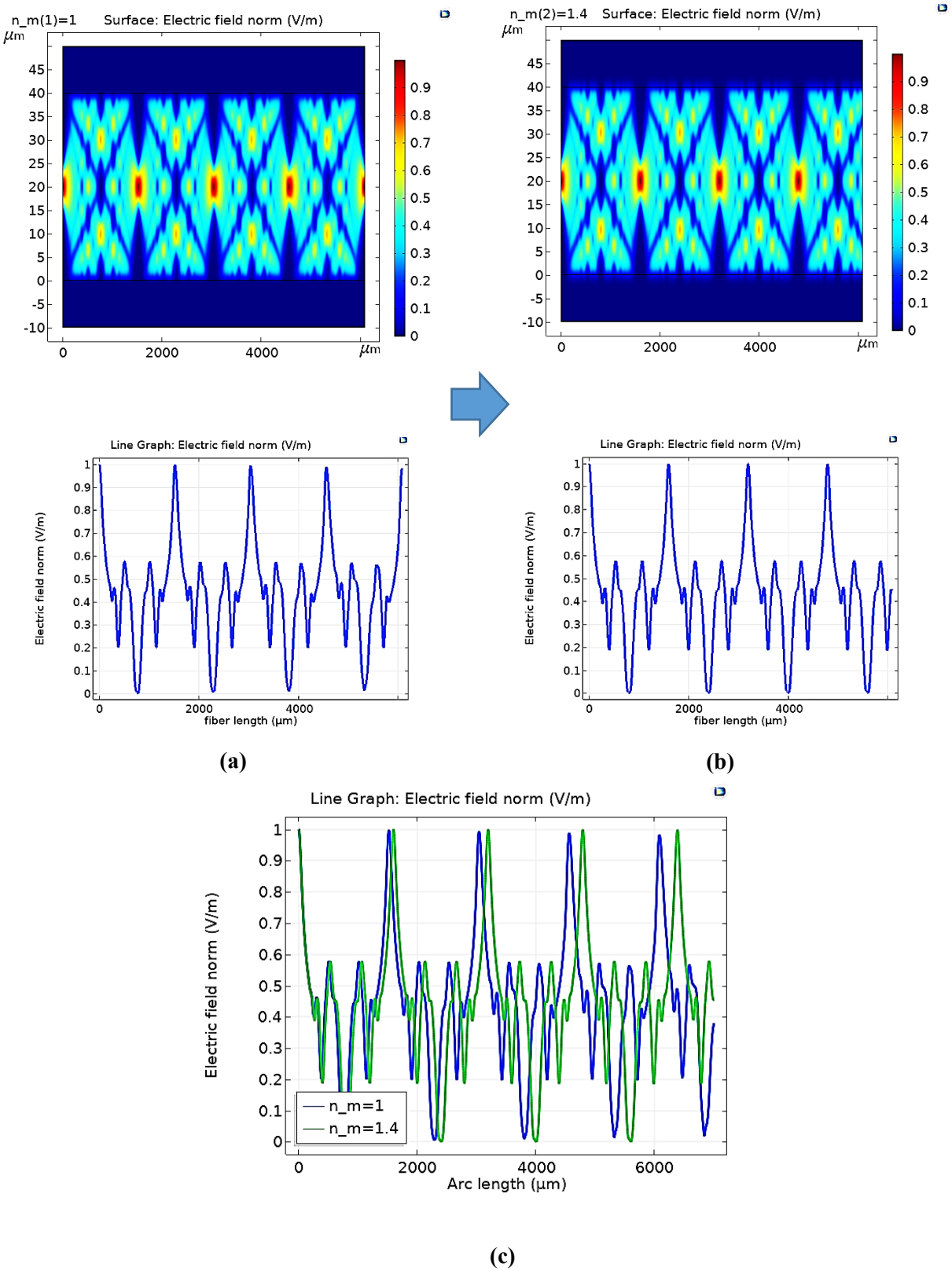

Figure 8: Visualizing the effect of ERI change on the position of the self-imaging, the MMI and the electric field illustrating the peaks of the self-imaging positions at (a) n_m = 1, (b) n_m = 1.4 (c) the field of both ERI

3.4 Self-imaging position at Different NCF lengths

The MMI in the cascaded SNS is shown in Figure 9 (a). The diameter and length of the studied NCF are 125 µm and 6 cm, and the wavelength is 1550 nm. The transverse field distribution illustrated in (b) at various lengths along the NCF is evaluated, at the input field L = 0, half of the first self-imaging L = 0.7425 cm, the first self-imaging length L=1.485 cm, and at L= 3 cm. The maximum intensity evaluated at L = 1.485 cm since it is the first self-imaging position. The intensity is varied along the NCF segment. The length of the NCF is important in the transmitted intensity and the coupling loss. The field distribution in the cross-section is symmetric as only LP_{0n} modes are excited in the MMI fiber structure.

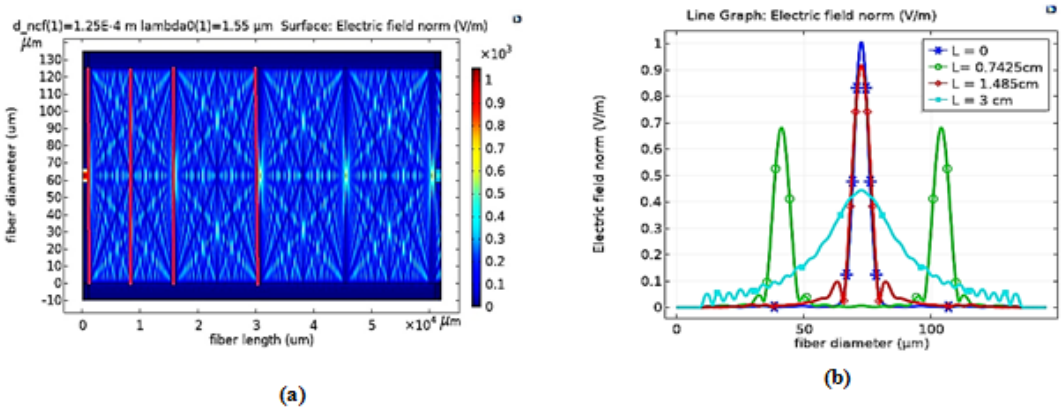

Figure 9: (a) The MMI of the cascaded SNS, (b) the transverse field distribution at different lengths along the NCF. The red lines in (a) illustrate the lengths at which the field studied transversely

3.5 Tunable fiber filter

The electric field along the NCF for the wavelengths 1530, 1540, 1550, 1560, and 1570 nm is studied. The NCF length is 2.5 cm, and the diameter is 80 µm. Figure 10 (a) illustrates that each wavelength has a certain self-imaging position. The coupled out wavelength shifts when the NCF length varies, as shown in eq. (4). Changing the NCF length to about 0.6 mm produce a wavelength shift of about 40 nm, about 10 nm each 150 µm elongation in the NCF length. The self-imaging position is not varied with the NCF length. The transmitted intensity and the wavelength are changed, which is the base of fiber sensors and the tunable fiber filters. Table 4 summarizes the relationship between the increment in the studied parameters with the self-imaging length.

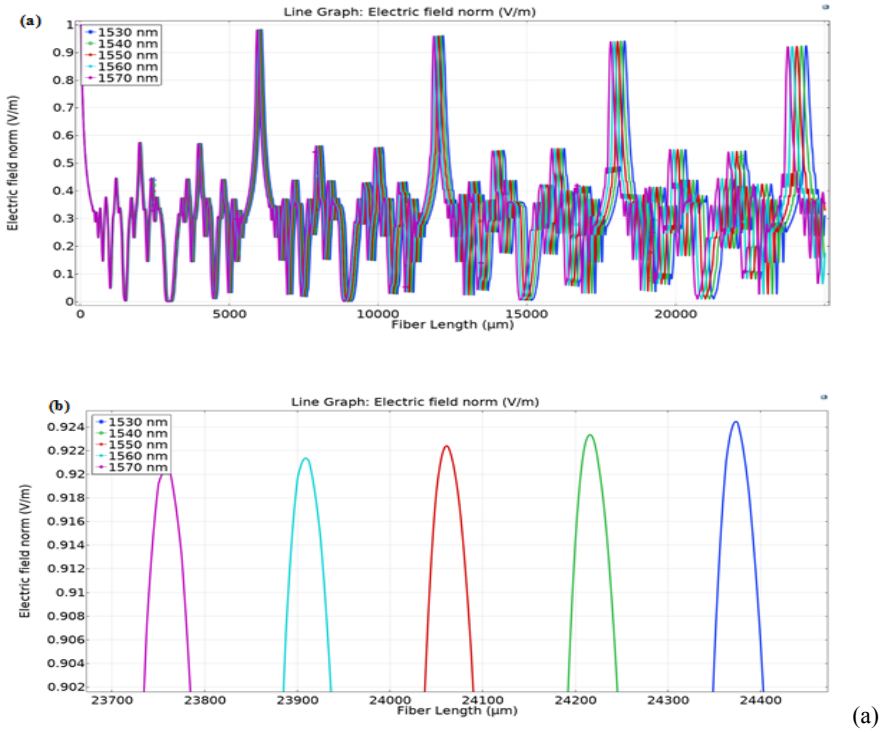

Figure 10: The electric field propagation along the NCF for the wavelengths 1530, 1540, 1550, 1560, and 1570 nm. (b) enlarged peaks of the propagated wavelengths

Table 1: The studied parameters with the self-imaging length

The studied parameter	Self-imaging length	Cause
Propagated Wavelength	Decrease	decreasing the number of the excited modes in the NCF
NCF Diameter	Increased	increasing the number of the excited modes in the NCF
ERI	Increased	Penetration depth enhanced
NCF Length	Not affected	Only the coupled out intensity and wavelength varied

4. Conclusions

The self-imaging in cascaded optical fiber at different NCF specifications and propagating wavelength is simulated using finite element beam envelope method by Comsol Multiphysics, 5.5. The results show that it is not necessary to be restricted to the rule of P = 4, 8... to get high self-imaging quality. The self-imaging quality is higher, about 0.9, for a small NCF diameter. The self-imaging length increased with a large NCF diameter and decreased with a longer wavelength, and it is increased with the increase in ERI. The NCF length is important in determining the coupled out intensity and wavelength. The field in the cascaded fiber is simulated for single and multi-wavelengths to evaluate the maximum transmission and study the structure's tunability. The BEM is suitable for simulating the field in large guiding photonic devices, representing different applications' bases as a tunable filter and fiber sensor.

Author contribution

All authors contributed equally to this work.

Funding

This research received no specific grant from any funding agency in the public, commercial, or not-for-profit sectors.

Data availability statement

The data that support the findings of this study are available on request from the corresponding author.

Conflicts of interest

The authors declare that there is no conflict of interest.

References

[1] X. Ma, D. Chen, Q. Shi, G. Feng, J. Yang, Widely tunable thulium-doped fiber laser based on multimode interference with a large No-core fiber, J. Light. Technol., 32 (2014) 3234–3238.

[2] K. Zhang, I. Alamgir, M. Rochette, Midinfrared Compatible Tunable Bandpass Filter Based on Multimode Interference in Chalcogenide Fiber, J. Light. Technol., 38 (2020) 857–863.

[3] R. Tamayo, J. Soto, M. Sánchez, MMI filters configuration for dual-wavelength generation in a ring cavity erbium-doped fibre laser, J. Eur. Opt. Soc., 12 (2016) 5. https://doi.org/10.1186/s41476-016-0025-5

[4] J. K. Hmood, New Design of Optical Filters Based on Single Mode-Multimode-Single Mode Fiber Structure for Optical Fiber Communication Systems, Eng. Tech. J., 29 (2011) 3172–3184. http://dx.doi.org/10.30684/etj.29.15.11

[5] N. Irawati, A. M. Hatta, Y. G. Y. Yhuwana, Sekartedjo, Heart Rate Monitoring Sensor Based on Singlemode-Multimode-Singlemode Fiber, Photonic. Sens., 10 (2020) 186–193. http://dx.doi.org/10.30684/etj.29.15.11

[6] F. S. Al-thahapy , A. A. Al-dergazly, Tuneable Photonic Fiber Bragg Grating for Magnetic Field Sensor, Preprints, (2016). http://dx.doi.org/10.20944/preprints201611.0088.v1

[7] J. K. Hmood, Novel Optical Fiber Sensor Based on SGMS Fiber Structure for Measuring Refractive Index of Liquids and Gases, IRAQI , J. Appl. Phys., 7 (2011) 17–21.

[8] L. B. Soldano , E. C. Pennings, Optical Multi-Mode Interference Devices Based on Self-Imaging : Principles and Applications, J. Light. Technol., 13 (1995) 615, 1995. http://dx.doi.org/10.1109/50.372474

[9] S. W. Allison , G. T. Gillies, Observations of and applications for self-imaging in optical fibers, Appl. Opt., 33 (1994) 1802-1805. http://dx.doi.org/10.1364/AO.33.001802

[10] H. J. Baker, J. R. Lee, D. R. Hall, Self-imaging and high-beam-quality operation in multi-mode planar waveguide optical amplifiers, Opt. Express., 10 (2002) 297-302. http://dx.doi.org/10.1364/OE.10.000297

[11] X. Zhu, A. Schülzgen, H. Li, S. Suzuki, Single-transverse-mode output from a fiber laser based on multimode interference, Opt. Lett., 33 (2008) 908-910. http://dx.doi.org/10.1364/OL.33.000908

[12] R. Selvas, I. T. Gomez, A. M. Rios, Wavelength tuning of fiber lasers using multimode interference effects, Opt. Express., 13 (2005) 9439–9445. http://dx.doi.org/10.1364/OPEX.13.009439

[13] X. Lian, Q. Wu, G. Farrell, C. Shen, Y. Ma, Y. Semenova, Discrete Self-Imaging in Small-Core Optical Fiber Interferometers, J. Light. Technol., 37 (2019). 1873–1884. http://dx.doi.org/10.1109/JLT.2019.2894365

[14] J. Yu, J. Zhang, Q. Shenga, All-fiber CW optical parametric oscillator tuned from 1642.5 to 1655.4 nm by a low-loss SMS filter, Results Phys., 17(2020) 103136. https://doi.org/10.1016/j.rinp.2020.103136

[15] F. Mangini, M. Ferraro, M. Zitelli, A. Niang, Experimental observation of self-imaging in SMF-28 optical fibers, Opt. Express., 29 (2021) 12625 . http://dx.doi.org/10.1364/OE.419472

[16] O. Shulika , I. Sukhoivanov, Advanced Lasers Laser Physics and Technology for Applied and Fundamental Science, ed. Mexico: springer, (2015). https://doi.org/10.1007/978-94-017-9481-7

[17] K. Tian, G. Farrell, X. Wang, Y. Xin, High sensitivity temperature sensor based on singlemode-no-core-singlemode fibre structure and alcohol, Sens. Actuator. A Phys., 284 (2018) 28–34. https://doi.org/10.1016/j.sna.2018.10.016

[18] J. Zheng, J. Li, T. Ning, L. Pei, S. Jian, Y. Wen, Improved self-imaging for multi-mode optical fiber involving cladding refractive index, Opt. Commun., 311 (2013) 350–353. http://dx.doi.org/10.1016/j.optcom.2013.08.070

[19] Y. Raichlin , A. Katzir, Fiber-optic evanescent wave spectroscopy in the middle infrared, Appl. Spectrosc., 62 (2008) 55–72. http://dx.doi.org/10.1366/00037020 .8783575

[20] T. Mukai , H. Fukano, Multipoint refractive index measurement using multimode interference-based fiber-optic sensors driven by an integrable tunable laser assembly, Jpn. J. Appl. Phys., 59 (2020) 5. https://dx.doi.org/10.35848/1347-4065/ab9996

[21] P. Zhang, T. Wang, W. Ma, K. Dong, H. Jiang, Tunable multiwavelength Tm-doped fiber laser based on the multimode interference effect, Appl. Opt., 54 (2015) 4667-4671. https://doi.org/10.1364/AO.54.004667

[22] Y. Zhou, S. Lou, Z. Tang, T. Zhao, W. Zhang, Tunable and switchable C-band and L-band multi-wavelength erbium-doped fiber laser employing a large-core fiber filter, Opt. Laser. Technol., 111 (2019) 262–270. https://doi.org/10.1016/j.optlastec.2018.09.042

[23] A. C. Guzman, J. E. A. Lopez, R. S. Aguilar, Widely tunable Erbium-doped fiber laser based on multimode interference effect, Opt. Express., 18 (2010) 591–597. https://doi.org/10.1364/OE.18.000591

[24] Q. Wang, G. Farrell, W. Yan, Investigation on single-mode-multimode-single-mode fiber structure, J. Light. Technol., 26 (2008) 512–519. http://dx.doi.org/10.1109/JLT.2007.915205

[25] S. Younus, A. Al-Dergazly, A. Abass, Characterization of Multimode Interference Based Optical FiberInt, Conf. Eng. Sci. Mater. Sci. Eng. dyala, 1076 (2021) 012060. http://dx.doi.org/10.1088/1757-899X/1076/1/012060

[26] Y. Mizuyama, How to Use the Beam Envelopes Method for Wave Optics Simulations, COMSOL Blog, 15 (2018) 27–29.

[27] X. Zhu, A. Schülzgen, H. Li, Detailed investigation of self-imaging in largecore multimode optical fibers for application in fiber lasers and amplifiers, Opt. Express, 16 (2008) 16632-16645. http://dx.doi.org/10.1364/OE.16.016632

[28] J. Zhao, J. Wang, C. Zhang, Refractive Index Fiber Laser Sensor by Using Tunable Filter Based on No-Core Fiber, IEEE Photonics. J., 8 (2016) 1–8. http://dx.doi.org/10.1109/JPHOT.2016.2609598

[29] Q. Meng, X. Dong, K. Ni, Y. Li, B. Xu, Z. Chen, Optical fiber laser salinity sensor based on multimode interference effect, IEEE Sens. J., 14 (2014) 1813–1816. http://dx.doi.org/10.1109/JSEN.2014.2298511

[30] M. Y. Elsayed, S. M. Sherif, A. S. Aljaber, d M. A. Swillam, Integrated lab-on-a-chip optical biosensor using ultrathin silicon waveguide SOI MMI device, Sensors., 20 (2020) 4955. http://dx.doi.org/10.3390/s20174955